JOURNAL OF SOLID STATE CHEMISTRY **124,** 338–345 (1996)
ARTICLE NO. 0247

Magnetic Structures of the 1D-Antiferromagnetic Fluorides Rb_2MnF_5 and $Rb_2MnF_5 \cdot H_2O$

P. Núñez*,[1] and T. Roisnel†

*Departamento de Química Inorgánica, Universidad de La Laguna, E-38200 La Laguna, Tenerife, Spain; and †Laboratoire Léon Brillouin (CEA-CNRS), CE Saclay, 91191 Gif sur Yvette Cedex, France

Received January 29, 1996; accepted April 10, 1996

Magnetic structures of the chain-based pentafluoromanganates(III) $Rb_2MnF_5 \cdot H_2O$ and Rb_2MnF_5 have been determined by means of neutron powder diffraction. Both compounds exhibit 3D antiferromagnetic order below $T_N = 22.0(2)$ K and $T_N = 26.0(5)$ K, respectively. Their identical magnetic structures are characterized by antiferromagnetic infinite chains of *trans*-corner connected octahedra $[MnF_4F_{2/2}]$, with antiferromagnetic ordering between the closest chains. The magnetic moment modulus on the Jahn–Teller Mn^{3+} ion has been found to be 3.14(14) μ_B and 3.30(10) μ_B, for the hydrate and anhydrous compounds, respectively. These relatively low values can be explained by a zero-spin reduction in antiferromagnetic low dimensional systems. The results are discussed in terms of relationships between structural and magnetic properties and compared with those obtained for others pentafluoromanganates (III).

I. INTRODUCTION

Structural and magnetic properties of chain-based Mn(III) pentafluorides have become a fascinating and productive area of research, mainly during the last decade (1–8). As was pointed out, the structural simplicity of this series of compounds makes them quasi-ideal to investigate detailed correlations between structural and magnetic properties (6). It is well established that Mn(III) has a strong tendency to exhibit $[MnF_6]^{3-}$ distorted octahedra due to the influence of the Jahn–Teller effect. This fact is intimately related to the tendency to form chains or layers of corner-sharing $[MnF_6]^{3-}$ octahedra.

It is possible to classify the chain-based pentafluoromanganates(III) as two types, hydrated and anhydrous compounds, depending on whether or not they have any water molecules of hydration. The hydrated group is formed by $A_2MnF_5 \cdot H_2O$ (A = K, Rb, Cs, Tl) and $AMnF_5 \cdot H_2O$ (A = Ba, Sr) and the anhydrous group by A_2MnF_5 (A = Li, Na, Rb, Cs, NH_4). Another classification of the pentafluoromanganates(III) that has been pointed out by Massa (7) depends on the arrangement of the chain packing in the crystal, hexagonal or tetragonal packing. A good example of the former group is given by $(NH_4)_2MnF_5$, whereas other members of the group must be called "pseudohexagonal" as in A_2MnF_5 (A = Li, Na), $A^{II}MnF_5 \cdot H_2O$ (A^{II} = Ba, Sr), and $K_2MnF_5 \cdot H_2O$. Examples of tetragonal chain packing are $A_2MnF_5 \cdot H_2O$ (A = Rb, Cs, Tl) and A_2MnF_5 (A = Rb, Cs).

In a previous paper (1), the magnetic properties of Rb_2MnF_5 and $Rb_2MnF_5 \cdot H_2O$, together with other alkaline-metal fluoromanganates(III), were reported. All of these compounds exhibit behavior which is characteristic of a low dimensional antiferromagnetic system. The intrachain exchange constants J/k have been determined by fitting the magnetic susceptibility data to Fisher's equation (11) adapted by Smith and Friedberg (12) for finite chains with $S = 2$, and correspond to antiferromagnetic superexchange couplings. A clear correlation between the calculated J/k values and both corresponding Mn–F–Mn angles (inside the chains) and Mn–Mn distances (inside the chains) has been observed. As expected, J/k decreases for both increasing deviations of the Mn–F–Mn angles from 180° and increasing Mn–Mn distances (1). Also, a correlation between J/k and $\cos^2 \beta$ has been proposed, where β is the intrachain Mn–F–Mn angle (2). This phenomena can be explained by the decrease of the overlap between the orbitals that are responsible for superexchange interactions (d_{z^2} of the Mn^{3+} ion and p of fluorine).

The crystal structure of $Rb_2MnF_5 \cdot H_2O$ has been determined (9) by X-ray diffraction and a topotactical dehydration study has been carried out on single crystals (10). In the present work, we describe the preparation of the Rb_2MnF_5 compound and its crystal and magnetic structures, determined from a neutron powder diffraction study, as well as the magnetic structure of $Rb_2MnF_5 \cdot H_2O$. Both magnetic structures are compared with those of other pentafluoromanganates(III).

[1] To whom all correspondence should be addressed.

0022-4596/96 $18.00

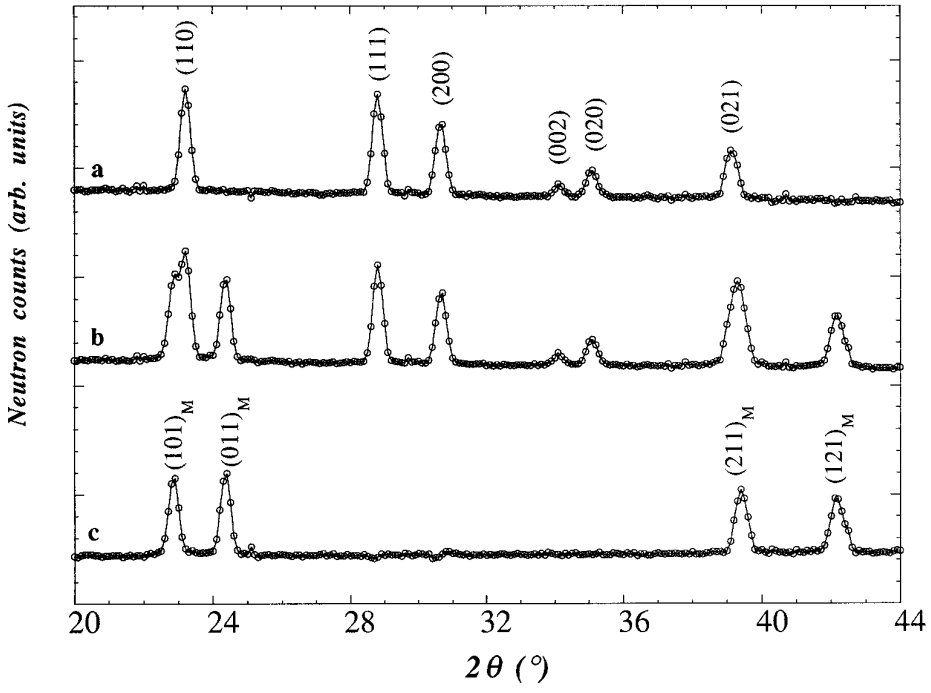

FIG. 1. Neutron diffraction patterns of $Rb_2MnF_5 \cdot H_2O$ at 30.6 K (a) and 1.5 K (b); difference pattern (c) [the $(hkl)_M$ indexing is given in the magnetic unit cell].

II. EXPERIMENTAL

Sample Preparations

$Rb_2MnF_5 \cdot H_2O$ was prepared as described elsewhere (9) by Bukovec *et al.* and confirmed by X-ray diffraction. The Rb_2MnF_5 compound was obtained by dehydration under vacuum of the hydrate in an alumina container at 130°C for 3 h. All manipulations were carried out in a dry box in order to avoid rehydration.

Neutron Diffraction

Neutron diffraction measurement were performed at the Orphée reactor (Saclay, France) on the 3T2 high resolution powder diffractometer ($\lambda = 1.2259$ Å) for the determination of the nuclear structure of Rb_2MnF_5 and on the 2 axis diffractometer G4.1 ($\lambda = 2.426$) (13) for the determination of the magnetic structures of both hydrated and anhydrous compounds. The anhydrous powder sample was sealed in an airtight vanadium container for the neutron experiments. Neutron data were analyzed with the Rietveld-type Fullprof program (14), using neutron scattering length from (15) and magnetic form factor of Mn^{3+} from (16).

III. RESULTS AND DISCUSSION

Magnetic Structure of $Rb_2MnF_5 \cdot H_2O$

Neutron diffraction patterns of $Rb_2MnF_5 \cdot H_20$ at 30.6 and 1.5 K are shown in Fig. 1, together with the corresponding difference pattern. The pattern recorded in the paramagnetic state at $T = 30.6$ K (Fig. 1a) exhibits only nuclear contributions and is in good agreement with the orthorhombic crystal structure determined by Bukovec *et al.* (9) (space group *Cmcm*, $a = 9.273(6)$ Å, $b = 8.115(4)$ Å, and $c = 8.344(4)$ Å). This structure can be described by the existence of infinite elongated octahedra $[MnF_4F_{2/2}]$ chains along the **c**-axis, separated by rubidium atoms and water molecules. In such a base-centered unit cell, the manganese atoms are located in a (4*a*) crystallographic site.

At $T = 1.5$ K (Fig. 1b), some superstructure peaks are observed in the neutron pattern, which are attributed to the appearance of magnetic ordering, and can be indexed to a primitive orthorhombic unit cell. These pure magnetic Bragg peaks are labeled (101), (011), (211), and (121) (Fig. 1c). The loss of the C lattice results in the following magnetic selection rule: $h + k = 2n \pm 1$. This antitranslation leads to an antiferromagnetic arrangement between magnetic moments located on atoms which are separated by the $(\frac{1}{2}\ \frac{1}{2}\ 0)$ translation, that is $\mathbf{Mn}_1$ (0 0 0) and $\mathbf{Mn}_3$ $(\frac{1}{2}\ \frac{1}{2}\ 0)$ on one side and $\mathbf{Mn}_2$ $(0\ 0\ \frac{1}{2})$ and $\mathbf{Mn}_4$ $(\frac{1}{2}\ \frac{1}{2}\ \frac{1}{2})$ on the other side. The best fitting of these observed magnetic Bragg peaks by a profile type refinement (14) has been obtained with magnetic moments parallel to the **c**-axis (chains axis) and with the following sequence: $+\mathbf{Mn}_1 - \mathbf{Mn}_2 - \mathbf{Mn}_3 + \mathbf{Mn}_4$. That means that in addition to the antiferromagnetic interchain interactions (antitranslation), there is an antiferromagnetic arrangement between the manganese moments inside the infinite chains (Fig. 2).

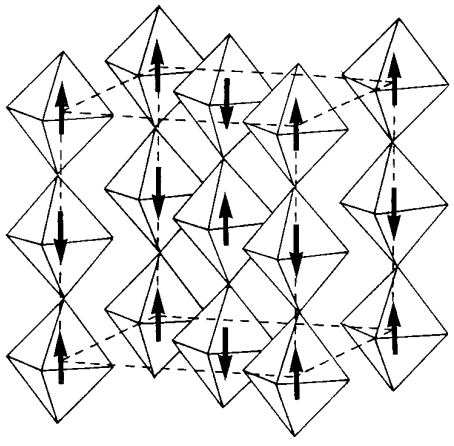

FIG. 2. Magnetic structure of $Rb_2MnF_5 \cdot H_2O$.

No change in this magnetic structure has been observed with temperature in the ordered magnetic state. The thermal evolution of the integrated intensity of the magnetic Bragg peaks is plotted in Fig. 3 and leads to an ordering temperature of $T_N = 22.0(5)$ K. At 1.5 K, the magnetic moment per manganese atom, as calculated from the magnetic structure model described above, is equal to 3.14(14) μ_B and is in good agreement with those observed for other Mn(III) fluorides ($S = 2$) in a low dimensional arrangement (3, 8).

Nuclear Structure of Rb_2MnF_5

Rb_2MnF_5, which was obtained from $Rb_2MnF_5 \cdot H_2O$ by a dehydration process, has a tetragonal $P4/mmm$ space group with the lattice parameters at room temperature $a = 6.0971(6)$ Å and $c = 4.1331(5)$ Å, which are in good agreement with those obtained from X-ray diffraction data (10). Rietveld profile refinement of the neutron data recorded at room temperature (Fig. 4) has been performed (with the reliability factors $R_p = 4.77\%$, $R_{wp} = 5.65$ and $\chi^2 = 1.95$) with the atomic positions and anisotropic Debye–Waller thermal factors listed in Table 1. We can note that in the $P4/m$ space group, which has also been proposed for this compound by Günter *et al.* (10), the F_1 atom is located in the ($4j$) crystallographic site, that is in a (x y 0) position. Refinement of these x and y coordinates leads to identical values, within the estimated standard deviations. Therefore, Rb_2MnF_5 can be refined in the $P4/mmm$ space group.

The structure of Rb_2MnF_5 consists of infinite chains of *trans*-corner connected octahedra $[MnF_4F_{2/2}]$ running parallel to the **c**-axis (Fig. 5), which are packed in a tetragonal way. The $[MnF_6]$ octahedra show a ferrodistortive ordering and exhibit as usual a strong elongation in the chain direction ($4 \times Mn–F_1 = 1.8514(36)$ Å and $2 \times Mn–F_2 = 2.0666(3)$ Å) (Table 1). This distortion can be largely attributed to the Jahn–Teller effect of Mn(III) in the high-spin d^4 configuration. The bridging Mn–F–Mn angle within the chains is linear (180°) in this compound. The Rb atoms are located between the chains for charge balance and are in a 10 coordination polyhedron ($8 \times Rb–F_1 = 3.00$ Å and $2 \times Rb–F_2 = 3.05$ Å).

The relationship between the cell parameters of the hydrated phase, $Rb_2MnF_5 \cdot H_20$ and the anhydrous phase Rb_2MnF_5 could be evaluated as

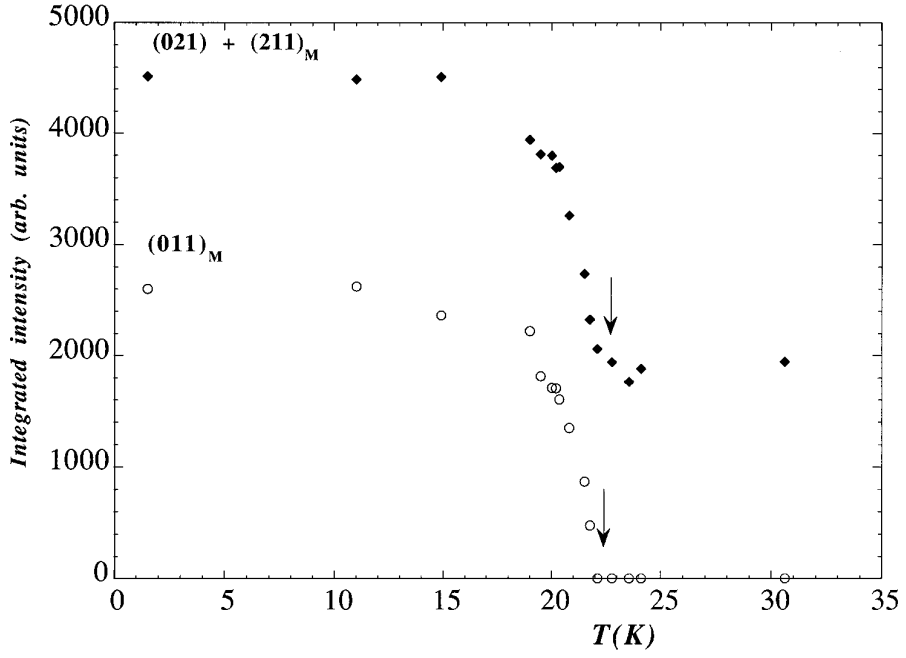

FIG. 3. Thermal variation of the integrated intensity of some magnetic Bragg peaks in $Rb_2MnF_5 \cdot H_2O$. The arrows indicate the Néel temperature (T_N).

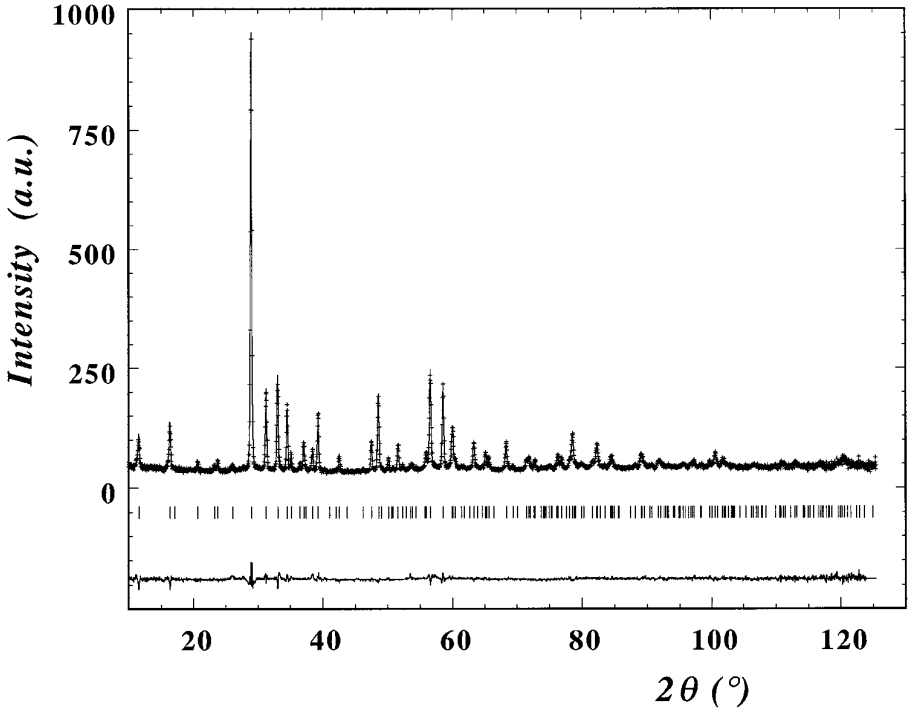

FIG. 4. Neutron diffraction patterns of Rb_2MnF_5 at room temperature (T = 300 K (3T2)) (λ = 1.2259 Å). (a) experimental points; continuous lines: calculated profile; (b) position of the nuclear peaks; (c) difference pattern.

$$a_t \approx a_o \cdot \sqrt{2} \approx b_o \cdot \sqrt{2}$$

$$c_t \approx c_o,$$

where the subscript t refers to the tetragonal lattice and o refers to the orthorhombic lattice.

At the same time that water molecules are removed from the structure of $Rb_2MnF_5 \cdot H_2O$, a tilting of the octahedra is required to stabilize the anhydrous structure. A topotactical study has been carried out on the dehydration process on this system (10) and also on the homologous system $Cs_2MnF_5 \cdot H_2O/Cs_2MnF_5$ (18). The dehydration–rehydration mechanism observed for both compounds is a reversible process and can be interpreted on the basis of a topotactical reaction: position and direction of the chains are affected only very little by the removal/introduction of water molecules in the unit cell. This is illustrated in our study (dehydration of the $Rb_2MnF_5 \cdot H_2O$ compound) by the following structural features: (i) conservation of the tetragonal chain packing; (ii) very small change of the Mn–F–Mn angle, from 176° to 180°, leading to completely linear chains in the Rb_2MnF_5 compound.

TABLE 1
Cell Parameters, Atomic Positions, Anisotropic Thermal Parameters (×10⁴), and Selected Distances (Å) and Angles (°) of Rb_2MnF_5 Determined from Refinement of Room Temperature Neutron Diffraction Data (3T2 Instrument)

Tetragonal s.g. $P4/mmm$ (No. 123): a = 6.0971(6) Å, c = 4.1331(5) Å; V = 153.66(5) Å^3

Atom	Site	x	y	z	β_{11}(Å^2)	β_{22}(Å^2)	β_{33}(Å^2)	β_{12}(Å^2)	β_{13}(Å^2)	β_{23}(Å^2)
Rb	2*e*	0.5	0	0.5	96(6)	285(8)	198(15)	0	0	0
Mn	1*a*	0	0	0	92(9)	92(9)	46(25)	0	0	0
F_1	4*j*	0.2147(40)	0.2147(4)	0	138(4)	138(4)	322(14)	−43(10)	0	0
F_2	1*b*	0	0	0.5	226(9)	226(9)	14(20)	0	0	0

Mn–F_1 = 1.8514(36) Å; Mn–F_2 = 2.0666(3) Å, Mn–F–Mn = 180°

Note. The estimated standard deviations (e.s.d.) of the last significant digit is given in parentheses. Each e.s.d. has been multiplied by a factor 2.2, following reference (17).

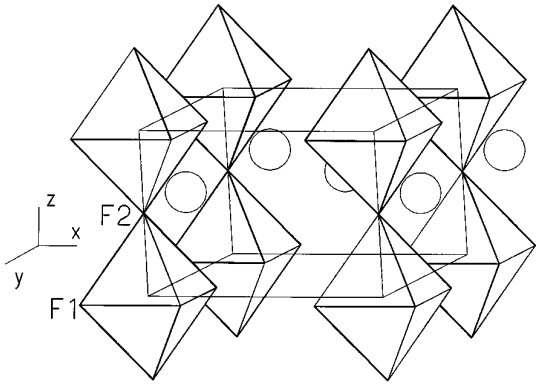

FIG. 5. Crystal structure of Rb_2MnF_5.

We have summarized in the Table 2 some structural data for several chain-based pentafluoromanganates, for the anhydrous and hydrated compounds, and indicated if they exhibit tetragonal or hexagonal chain packing.

Magnetic Structure of Rb_2MnF_5

Neutron diffraction patterns of the anhydrous compound Rb_2MnF_5 were recorded on the G41 diffractometer in the ordered magnetic state below 35 K. In the paramagnetic state (Fig. 6a) at $T = 35$ K, only nuclear contributions are observed and the neutron pattern is in good agreement with the crystal structure at room temperature described just before.

At $T = 1.5$ K, several magnetic superstructure Bragg peaks are observed (Fig. 6b), which can not be indexed in the crystallographic unit cell: a unit cell doubled in all three directions is required to index the observed peaks with integer (*hkl*) indices. As described in the previous paragraph, the manganese atom is located in the (1*a*) crystallographic site in the (**aac**) tetragonal unit cell. From this simple consideration, it is easy to deduce that the antiferromagnetic arrangement observed in the magnetic behavior (1) requires a cell larger than the nuclear (**aac**) one. The observed superstructure peaks can also be labeled as satellites of nuclear Bragg peaks with the propagation vector $\mathbf{k} = (\frac{1}{2}\,\frac{1}{2}\,\frac{1}{2})$, leading to an antiferromagnetic ordering in the three crystallographic directions.

The refinement of the neutron data with such a collinear antiferromagnetic structure leads to magnetic moments that are aligned along the **c**-axis, that is the chain axis. The thermal variation of the magnetic peaks integrated is plotted in Fig. 7, leading to a Néel temperature of $T_N = 26.0(3)$ K. At the lowest temperature ($T = 1.5$ K), the magnetic moment modulus is found to be equal to 3.30(10) μ_B per Mn^{3+} atom.

Discussion

The compound $Rb_2MnF_5 \cdot H_2O$ has been proposed as an ideal monodimensional magnetic system with magnetic ordering occurring below 2 K (6, 23). These claims, which are in disagreement with our experimental results, were based on ac susceptometer data collected in the 300–2 K temperature range, in which no ''signal'' in the out-of-phase magnetic susceptibility component was observed.

TABLE 2
Selected Structural Data of Chain-Based Pentafluoromanganates(III)

Compound	Intrachain Mn–F–Mn(°)	Intrachain Mn–Mn (Å)	Chains Packing[a]	Chains Parallel to[b]	Interchain Mn–Mn (Å)[c]	Ref.
			Hydrate fluorides			
$K_2MnF_5 \cdot H_2O$	163.3	4.09	H	**b**	2 × 5.9	19
$Rb_2MnF_5 \cdot H_2O$	176.0	4.17	T	**c**	4 × 6.16	9
$Cs_2MnF_5 \cdot H_2O$	180.0	4.25	T	**c**	4 × 6.51	20
$Tl_2MnF_5 \cdot H_2O$	179.0	4.17	T	**c**	4 × 6.28	3
$SrMnF_5 \cdot H_2O$	139.8	3.96	H	**b**	2 × 5.1 + 2 × 6.1 + 2 × 6.5	21
$BaMnF_5 \cdot H_2O$	147.7	4.09	H	**b**	2 × 5.4 + 2 × 6.3 + 2 × 6.6	21
			Anhydrous fluorides			
Li_2MnF_5	121.5	3.70	H	**c**	2 × 4.9 + 4 × 5.59	2
Na_2MnF_5	132.5	3.86	H	**a**	2 × 5.2 + 4 × 6.0	7
$(NH_4)_2MnF_5$	143.4	3.97	H	**b**	6 × 6.20	22
Rb_2MnF_5	180	4.12	T	**c**	4 × 6.09	this work
Cs_2MnF_5	180	4.23	T	**c**	4 × 6.42	18

[a] Pseudohexagonal (H) or tetragonal (T) chain packing
[b] Chains running parallel to the indicated axis.
[c] Closest interchain Mn-Mn distances.

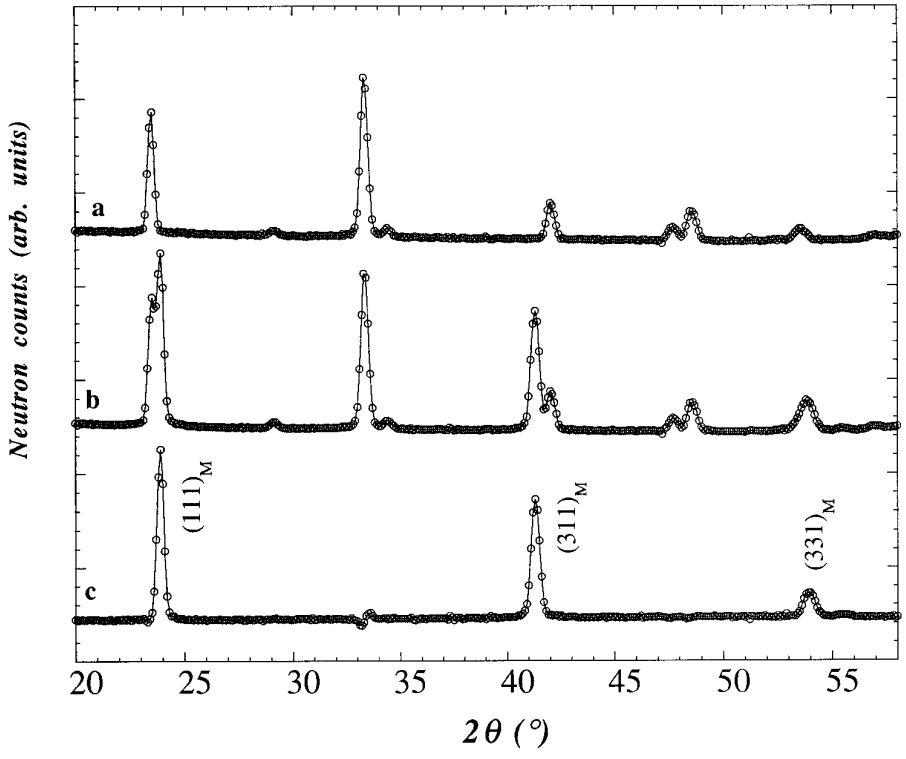

FIG. 6. Neutron diffraction pattern of Rb_2MnF_5 at 35 K (a) and 1.5 K (b); difference pattern (c) [the $(hkl)_M$ indexing is given in the magnetic unit cell].

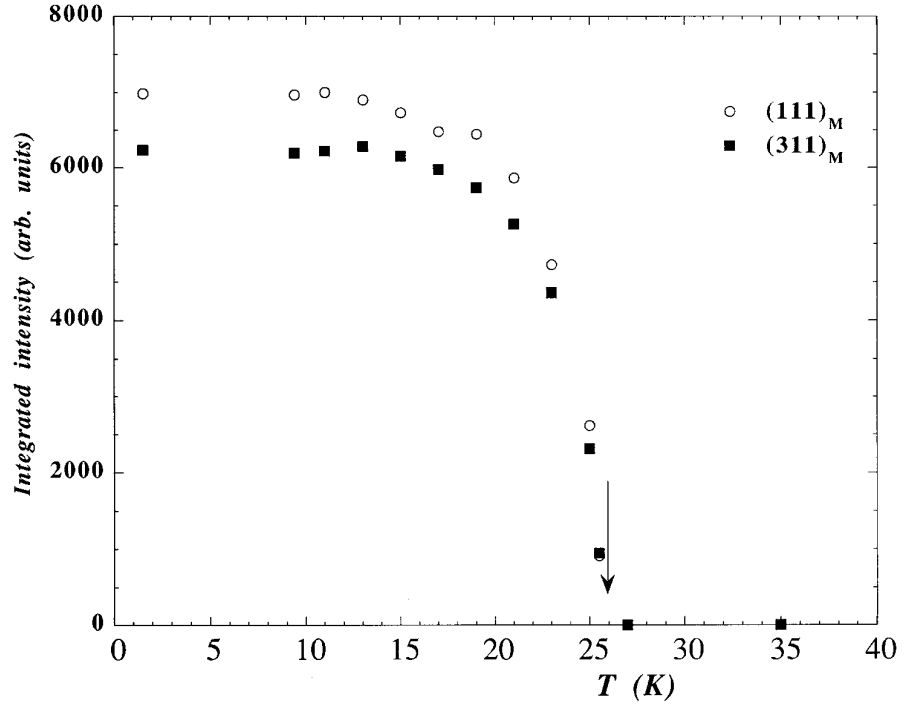

FIG. 7. Thermal variation of the integrated intensity of the (111) and (311) magnetic Bragg peaks in Rb_2MnF_5. The arrow indicates the Néel temperature (T_N).

TABLE 3
Selected Magnetic Data of Chain-Based Pentafluoromanganates(III)

Compound	θ_n(K)	C_n(exp.)	J/k (K)	g	T_N (K)[a]	Magnetic moments		Propagation vector	J/J'[c]	Ref.
						Modulus	Direction			
$K_2MnF_5 \cdot H_2O$	−295	3.95	−18.2	2.06						1
	−124		−15.5	1.95	17.6[b]					23
					17	3.33(5)	**b** axis	0 0 ½[d]	5×10^{-3}	24
$Rb_2MnF_5 \cdot H_2O$	−445	4.54	−21.8	2.09						1
	−428		−20.0	2.02						2
	−164		−20.5	1.84						23
					22.0(2)	3.14(14)	**c** axis	1 0 1	4×10^{-3}	this work
$Cs_2MnF_5 \cdot H_2O$	−360	4.41	−17.9	2.04						1
	−331		−19.0	2.01						2
$Tl_2MnF_2 \cdot H_2O$	−470	4.30	−21.5	1.99	28(1)	3.2(2)	**c** axis	1 0 1	2×10^{-3}	3
$SrMnF_5 \cdot H_2O$	−134		−10.3	1.88						2
$BaMnF_5 \cdot H_2O$	−181		−13.5	1.95						2
Li_2MnF_5	−66		−6.3	2.05					$<10^{-3}$	2
			−5.6	1.97						25
Na_2MnF_5	−91		−8.25	1.84						2
			−9.2	1.92						25
	−98	3.1	−8.6	1.95	11.1(5)	3.3(1)	**a** axis	0 ½ 0	3×10^{-2}	8
$(NH_4)_2MnF_5$			−10.6	1.93						25
	−153		−11.2	1.93						2
	−83.6		−10.45	2.02	5.2[b]				1×10^{-3}	23
Rb_2MnF_5	−400	4.29	−22.6	2.10						1
					26.0(3)	3.30(10)	**c** axis	½ ½ ½	8×10^{-3}	this work
Cs_2MnF_5	−345	4.29	−19.4	2.06						1

[a] Néel temperature from neutron diffraction data.
[b] Néel temperature from magnetic data.
[c] Oguchi's method (26).
[d] Cell parameters: $a < c$ (24).

But if no canting between the magnetic moments is present, then the out-of-phase magnetic susceptibility should be negligible and, consequently, the 3D magnetic ordering could not be detected by this technique.

The neutron diffraction studies presented in this paper show that Rb_2MnF_5 and $Rb_2MnF_5 \cdot H_2O$ both undergo 3D antiferromagnetic order at low temperature ($T <$ 22.0(6) and 26.0(3) K, respectively). In Table 3 we have listed some magnetic parameters (Curie–Weiss temperature θ, experimental Curie constant C_m(exp.), intrachain exchange energy J/k, Landé factor g, Néel temperature T_N, intrachain-to-interchain exchange constants ratio J/J', and magnetic structure description) of the rubidium compounds, as well as those of other pentafluoromanganates(III).

Both intrachain Mn–Mn distances and Mn–F–Mn angles (Table 2) are intimately related to the value of the corresponding intrachain exchange constant, J/k (Table 3) (1).

From Table 2 and 3, it is possible to deduce that (i) the moments of Mn(III) lie in the same direction as the chains, at least for the compounds whose data are available; (ii) as expected, the shortest interchain Mn–Mn distances are directly related to the direction in which the interchain magnetic interactions occur; and (iii) for the hydrated compounds, the Néel temperature, T_N, tends to increase as the magnitude of $|J/k|$ increases. This trend is not observed by the anhydrous compounds.

Magnetic structures of these compounds are in fact very similar (Fig. 8a and 8b) and present the same features as those of the known $Tl_2MnF_5 \cdot H_2O$ compound (3): (i) antiferromagnetic chains; (ii) antiferromagnetic interactions between closest chains ($d_{Mn-Mn} \approx 6.12$ Å); and (iii) magnetic moments aligned along the chains. Due to the fact that crystallographic unit cells are different between the two compounds, different propagation wave vectors ($\mathbf{k}$ = (1 0 1) in $Rb_2MnF_5 \cdot H_2O$ and $\mathbf{k}$ = (½ ½ ½) in the anhydrous compound) are needed to describe identical magnetic order. It can be also noted (see Table 3) that in both compounds the main interchain interactions are between first neighbor chains, unlike the Na_2MnF_5 compound, in which second neighbors interactions also takes place, leading to a frustration phenomena (Fig. 8c) (8).

The experimental values of the magnetic moment modu-

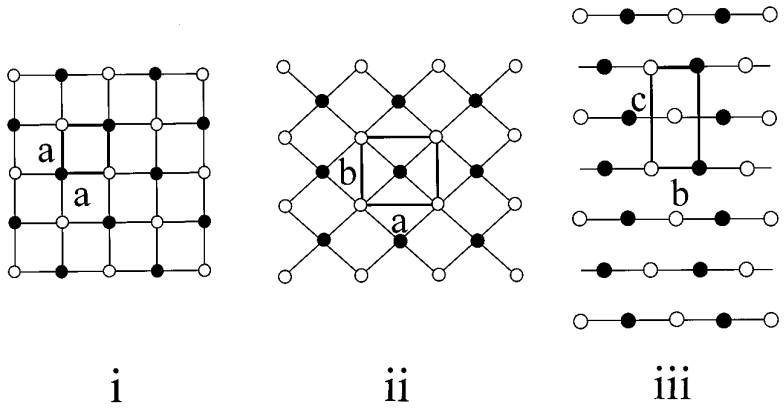

FIG. 8. Schematic representation of the magnetic structures of (i) Rb_2MnF_5, (ii) $Rb_2MnF_5 \cdot H_2O$, and (iii) Na_2MnF_5 in planes perpendicular to the antiferromagnetic chain axis. White and black circles represent antiferromagnetically coupled chains. Continuous lines are representative of the closest interchain Mn–Mn distances. The crystallographic unit cell is shown in bold lines.

lus for Mn(III) obtained for Rb_2MnF_5 and $Rb_2MnF_5 \cdot H_2O$ are lower than expected for a system with $S = 2$ (4 μ_B), but are in good agreement with the trend observed in other 1D pentafluoromanganates(III) (Table 3). This behavior is attributable to zero-point spin reduction which has been predicted to reduce the ground state spin expectation value in a low-dimensional antiferromagnetic system. This effect can be considered as a result of the zero-point energy of the spin waves destroying any long-range order (27, 28). A similar reduction of the magnetic moment value has been reported from a neutron diffraction study of the chain-based $Tl_2MnF_5 \cdot H_2O$ (3) and Na_2MnF_5 (8) compounds, which exhibit a magnetic moment of 3.2(2) μ_B and 3.3(1) μ_B at $T = 1.5$ K, respectively.

ACKNOWLEDGMENTS

The authors express their gratitude to Dr. Alain Tressaud (ICMCB, Université de Bordeaux I, France) for many fruitful discussions. Also, the authors thank Professor H. zur Loye and D. S. Trail (MIT, Cambridge, MA) for grammatical corrections.

REFERENCES

1. P. Núñez, J. Darriet, P. Burkovec, A. Tressaud, and P. Hagenmuller, *Mater. Res. Bull.* **22,** 661–667 (1987).
2. J. Pebler, W. Massa, H. Lass, and B. Ziegler, *J. Solid State Chem.* **71,** 87–94 (1987).
3. P. Núñez, A. Tressaud, J. Darriet, P. Hagenmuller, G. Hahn, G. Frenzen, W. Massa, D. Babel, A. Boireau, and J. L. Soubeyroux, *Inorg. Chem.* **31,** 770–774 (1992).
4. P. Núñez, A. Tressaud, W. Massa, D. Babel, A. Boireau, and J. L. Soubeyroux, *Phys. Status Solidi A* **127,** 505–517 (1991).
5. F. Palacio, M. Andrés, J. Rodriguez-Carvajal, and J. Pannetier, *J. Phys.: Condens. Matter* **3,** 2379–2390 (1991).
6. F. Palacio and M. C. Morón, "Research Frontiers in Magneto Chemistry" (C. J. O'Connor, Ed.), p. 227. Academic Press, Orlando, 1993.
7. W. Massa, *Acta Crystallogr. C* **42,** 644–647 (1986).
8. P. Núñez, T. Roisnel, and A. Tressaud, *Solid State Commun.* **92**(7), 601–605 (1994).
9. P. Bukovec and V. Kaûcic, *Acta Crystallogr. B* **34,** 3339–3341 (1978).
10. J. R. Günter, J. P. Matthieu, and H. R. Oswald, *Helv. Chim. Acta* **61,** 328–336 (1978).
11. M. E. Fischer, *Am. J. Phys.* **32,** 343 (1964).
12. T. Smith and S. A. Friedberg, *Phys. Rev.* **176,** 660 (1968).
13. T. Roisnel, J. Rodriguez-Carvajal, M. Pinot, G. André, and F. Bourée, *Mater. Sci. Forum* **166–169,** 245–250 (1994).
14. J. Rodriguez-Carvajal, "Abstracts of the Satellite Meeting on Powder Diffraction of the XV Congress of the IUcr," p. 127, Toulouse, France, 1991.
15. V. F. Sears, *Neutron News* **3**(3), 26 (1992).
16. P. J. Brown, "International Tables for Crystallography" (A. J. C. Wilson, Ed.), Vol. C, Table 4.4.4. Kluwer, Dordrecht, 1993.
17. J. F. Bérar and P. Lelann, *J. Appl. Crystallogr.* **24,** 1 (1991).
18. F. Hahn and W. Massa, *Z. Naturforsch. B* **45,** 1341–1348 (1990).
19. A. J. Edwards, *J. Chem. Soc. A,* 2653–2655 (1971).
20. V. Kaûcic and P. Bukovec, *Acta Crystallogr. B* **34,** 3337 (1978).
21. W. Massa and V. Burk, *Z. Anorg. Allg. Chem.* **516,** 119 (1984).
22. D. R. Sears and J. L. Hoard, *J. Chem. Phys.* **50**(3), 1066–1071 (1969).
23. M. Andrés, Thesis, University of Zaragoza, Spain, 1988.
24. T. Roisnel, P. Núñez, E. Molins, and A. Tressaud, to be published.
25. S. Emori, M. Inoue, M. Kishita, and M. Kubo, *Inorg. Chem.* **8,** 1385 (1969).
26. T. Oguchi, *Phys. Rev.* **133,** 1098 (1964).
27. G. P. Gupta, D. P. E. Dickson, C. F. Johnson, and B. M. Wanklyn, *J. Phys. C: Solid State Phys.* **10,** L459 (1977).
28. T. Ishikawa and T. Oguchi, *Prog. Theor. Phys.* **54,** 1282 (1975).